

Pion elastic scattering from polarized ^{13}C in the energy region of the P_{33} resonance

Yi-Fen Yen,^a B. Brinkmüller,^b D. Dehnhard, M. A. Franey, S. M. Sterbenz,^a
and Yi-Ju Yu^c

University of Minnesota, Minneapolis, Minnesota 55455

Brian Berman,^d G. R. Bureson, K. Cranston, A. Klein,^e and G. S. Kyle

New Mexico State University, Las Cruces, New Mexico 88003

R. Alarcon, T. Averett,^f J. R. Comfort, J. J. Görden,^g
B. G. Ritchie, and J. R. Tinsley^h

Arizona State University, Tempe, Arizona 85287

M. Barlett,ⁱ G. W. Hoffmann, K. Johnson, C. F. Moore, M. Purcell, H. Ward,
and A. Williams^j

University of Texas at Austin, Austin, Texas 78712-1081

J. A. Faucett, S. J. Greene, J. J. Jarmer, J. A. McGill,^k C. L. Morris,
S. I. Penttilä, and N. Tanaka^l

Los Alamos National Laboratory, Los Alamos, New Mexico 87545

H. T. Fortune, E. Insko, R. Ivie, J. M. O'Donnell,^m and D. Smith

University of Pennsylvania, Philadelphia, Pennsylvania 19104

M. A. Khandaker

University of Maryland, College Park, Maryland 20742

S. Chakravarti

California State Polytechnic University, Pomona, California 91768

(Received 21 December 1993)

Analyzing powers A_y were measured for π^+ and π^- elastic scattering from polarized ^{13}C at incident pion energies T_π near the P_{33} π -nucleon resonance. At $T_\pi = 130$ MeV, the values of A_y are significantly different from zero for π^- scattering. For π^+ at $T_\pi = 130$ MeV and for both π^- and π^+ at all other energies, the A_y are mostly consistent with zero. Elastic differential cross sections were measured using an unpolarized ^{13}C target. Both the analyzing-power and cross-section data were compared with predictions using a variety of nuclear structure and reaction models. The analyzing power was found to be strongly sensitive to the quadrupole spin-flip part of the transition. The data of this work complement measurements of the magnetic form factor by electron scattering. The pion

^aPresent address: Los Alamos National Laboratory, Los Alamos, NM 87545.

^bPresent address: Universität Karlsruhe, D-7500 Karlsruhe, Germany, and Paul Scherrer Institute, CH-5234 Villigen, Switzerland.

^cPresent address: Tandem Computers, Inc., 10100 N. Tantau Ave., Loc 251-01, Cupertino, CA 95014-0788.

^dPresent address: University of New Mexico, Albuquerque, NM 87131.

^ePresent address: Dept. of Physics, Old Dominion University, Norfolk, VA 23529.

^fPresent address: Dept. of Physics, University of Virginia, Charlottesville, VA 22901.

^gPresent address: Atlantic-Zeiser, Bogenstrasse 6-8, D-78576 Emmingen, Germany.

^hPresent address: EG&G/EM, 130 Robin Hill Road, Goleta, CA 93116.

ⁱPresent address: Applied Research Laboratory, University of Texas, Austin, TX 78713.

^jPresent address: Dept. of Physics, University of Pennsylvania, Philadelphia, PA 19104.

^kPresent address: MS 1049, SSC Laboratory, 2550 Beckleymeade Ave., Dallas, TX 75237.

^lDeceased.

^mPresent address: Dept. of Physics, University of Minnesota, Minneapolis, MN 55455.

A_y data are not reproduced by calculations using wave functions that fit the magnetic form factor at low momentum transfers.

PACS number(s): 24.70.+s, 25.80.Dj

I. INTRODUCTION

Since the advent of pion facilities, a large amount of elastic scattering data has been accumulated, particularly in the energy region of the P_{33} π -nucleon resonance, for studies of the π -nucleus interaction. These data, however, are insensitive to the spin-dependent part of the interaction. For example, the scattering amplitude of pion scattering from a spin- $\frac{1}{2}$ nucleus can be expressed as

$$t = \mathcal{F}(\theta) + i\mathcal{G}(\theta)\hat{n} \cdot \boldsymbol{\sigma}, \quad (1)$$

where $\boldsymbol{\sigma}$ is the nuclear Pauli spin matrix and $\hat{n} = (\mathbf{k} \times \mathbf{k}') / |\mathbf{k} \times \mathbf{k}'|$ with \mathbf{k} and \mathbf{k}' being the momenta of the incoming and outgoing pions. The quantities $\mathcal{F}(\theta)$ and $\mathcal{G}(\theta)$ are, respectively, the spin-independent and spin-dependent pion-nucleus scattering amplitudes. The former describes processes without a spin transfer ($\Delta S=0$) to the nucleus, whereas the latter involves a spin transfer ($\Delta S=1$). The differential cross sections $[d\sigma(\theta)/d\Omega]$,

$$d\sigma(\theta)/d\Omega = |\mathcal{F}(\theta)|^2 + |\mathcal{G}(\theta)|^2, \quad (2)$$

are dominated by $|\mathcal{F}(\theta)|^2$. A contribution from the small spin-dependent amplitude is difficult to observe in $d\sigma(\theta)/d\Omega$. However, the analyzing power

$$A_y(\theta) = \frac{2\text{Im}[\mathcal{F}(\theta)\mathcal{G}(\theta)^*]}{|\mathcal{F}(\theta)|^2 + |\mathcal{G}(\theta)|^2}, \quad (3)$$

is an interference term between $\mathcal{F}(\theta)$ and $\mathcal{G}(\theta)$, and thus can be very sensitive to spin effects.

Because large nuclear polarizations can now be achieved by the dynamic nuclear polarization (DNP) technique, it has become feasible to study A_y in pion scattering from nuclear targets [1–3]. In first order, the $\Delta S=1$ transition involves only one of the A nucleons in the target nucleus [1] but the $\Delta S=0$ transition involves all nucleons coherently. Therefore, the relative $\Delta S=1$ contribution is roughly proportional to A^{-1} , and the analyzing powers are predicted to be reasonably large for light nuclei. The inclusion of second-order terms in the theoretical calculations [4, 5] produces larger changes in the predicted A_y than in $d\sigma(\theta)/d\Omega$. Thus, measurements of A_y should allow sensitive tests of π -nucleus interaction models that include medium modifications of the free π -nucleon interaction in nuclei.

For the first A_y measurements, light nuclei were chosen. At the Paul Scherrer Institute (PSI) large analyzing powers were measured for elastic and inelastic $\pi^+ - {}^6\text{Li}$ scattering [6, 7]. Measurements by the same group [6, 8] on ${}^{15}\text{N}(\pi^+, \pi^+)$ at $T_\pi = 164$ MeV revealed surprisingly small analyzing powers, in sharp contrast to the large values predicted by theory.

We chose ${}^{13}\text{C}$ as a target nucleus to study spin effects in pion-nucleus elastic scattering because a polarized ${}^{13}\text{C}$ target had been developed with a sufficiently large po-

larization ($\sim 28\%$). In addition, experimental data exist for elastic and inelastic scattering of pions [9–11], electrons [12], and protons [13, 14] from ${}^{13}\text{C}$, and extensive analyses of these data have been made using theoretical nuclear wave functions [15, 16]. Scattering experiments with different probes elucidate different aspects of the nuclear structure and reaction mechanisms. Analyzing powers for ${}^{13}\text{C}(\pi^\pm, \pi^\pm)$ have recently been measured [17] at the Tri-University-Meson Facility at 100 MeV, i.e., lower than the energies of the current experiment.

The pion-nucleus interaction is especially sensitive to the isoscalar part of the transition density. Thus the present data complement electron-scattering measurements of the (isovector-dominated) magnetic form factor. However, by measuring both π^+ and π^- scattering, we also obtain information on the isovector terms. Values of A_y for the purely isovector reaction ${}^{13}\text{C}(\pi^+, \pi^0)$ to the ${}^{13}\text{N}$ ground and excited states were measured in another experiment [18] at the Clinton P. Anderson Meson Physics Facility (LAMPF).

Some of the data discussed in this paper have been published previously [19]. In the present paper we report in detail the results of both A_y and $d\sigma/d\Omega$ measurements on pion elastic scattering from polarized and unpolarized ${}^{13}\text{C}$ between $T_\pi = 114$ MeV and about 230 MeV. The experiment was carried out in the low-energy-pion (LEP) channel at LAMPF. The experimental techniques and the data reduction are described in Sec. II. Experimental results are compared with theoretical calculations using currently available reaction and nuclear structure models in Sec. III. A summary is given in Sec. IV.

II. EXPERIMENT

A. Polarized target

The ${}^{13}\text{C}$ nuclei were polarized using the DNP method [2, 3]. It requires cooling the target to about 0.5 K, applying a strong magnetic field (of the order of a few T) that is homogeneous throughout the volume of the target, and irradiating the target by microwaves which transfer the high electron polarization to the ${}^1\text{H}$ and ${}^{13}\text{C}$ nuclei. The target material was 99% ${}^{13}\text{C}$ -enriched 1-butanol (${}^{13}\text{C}_4\text{H}_{10}\text{O}$) mixed with 5% H_2O in volume. Polarization centers for DNP were created by doping the butanol with a paramagnetic complex EHBA-Cr(V) to the level of 5.2×10^{19} spin/cm³. A detailed description of the preparation of the target is given in Ref. [2].

The butanol was in the form of 1-mm diameter frozen beads contained in a cylindrical Teflon cell of 1-cm thickness and 2.54-cm diameter. The packing factor was about 70%. The axis of the cylinder was oriented at a fixed angle of 40° to the axis of the LEP channel in the scattering plane (Fig. 1). The Teflon cell was placed inside a copper microwave cavity and immersed in liquid ${}^3\text{He}$ at 0.5 K

supplied by an evaporation refrigerator. The total areal density of all materials in the target and target cell was about 0.76 g/cm^2 .

A conventional C magnet provided a 2.5-T magnetic field transverse to the scattering plane at the target. The C magnet had a gap width of 10.2 cm and an effective field boundary at a radius of 22.7 cm. The field homogeneity over the target volume was better than 4×10^{-4} . The small polarizations of the ^1H and ^{13}C nuclei in the butanol, due to the presence of the high magnetic field and the low temperature, were enhanced significantly by irradiating the sample with microwaves of a frequency of about 70 GHz. The orientation of the target polarization was reversed approximately every 2 h by a small change (0.43 GHz) in the microwave frequency. The polarizations of both the ^{13}C and ^1H nuclei were measured by a nuclear magnetic resonance (NMR) system using a small coil of thin copper wire that was placed inside the target cell.

The NMR measurements were calibrated by measuring periodically the small thermal-equilibrium (TE) signals from the target near 1 K. When the target was being irradiated by the microwaves, the polarizations of ^{13}C and ^1H nuclei reached average values of 0.28 and 0.82, respectively, within about 45 min. The ratio of the measured ^1H and ^{13}C polarizations agreed within the error bars with that expected from the equal-spin-temperature hypothesis [20]. *Relative* uncertainties of the polarizations were estimated to be 1.8% for ^1H and 2.9% for ^{13}C . These values include the statistical errors from the NMR spectra in the TE measurements and systematic errors from the temperature calibrations, the biases in the base line of the NMR spectra, and nonlinearities in the electronics.

B. Pion beam

Pion beam currents were typically $1.5 \times 10^7/\text{sec}$ for π^+ and $0.4 \times 10^7/\text{sec}$ for π^- . An ionization chamber (IC) in the pion beam upstream of the target (Fig. 1) was used to measure the relative pion beam current. Downstream from the target, a split ionization chamber (SIC) was placed to intercept the transmitted pions. The current from each of the right and left cells of the SIC was integrated and scaled. In addition, the primary 800-MeV proton-beam current, monitored by two toroidal coils near the pion-production target, was recorded. All of the

above beam related quantities and additional detector related quantities were recorded every 20 sec to monitor the experimental conditions during data acquisition.

In the process of data analysis, a series of tests was performed to constrain the selection of good events. One of these tests was placed on the scalers which monitored the SIC, IC, and the toroidal coils. Changes in the ratios of the monitor scalers provide information on beam instability and variations in the target composition, e.g., a change in the amount of liquid ^3He in the cavity. Events from time periods during which the scaler ratios were not within the test limits were excluded from further data analysis. A typical width of the test limits was as narrow as $\pm 1\%$ of the average scaler ratio. Approximately 10% of the data were excluded by these tests on the monitor scalers.

The high magnetic field in the region of the target bends the trajectories of the incoming and outgoing pions significantly (Fig. 1). A steering magnet, 1.37 m upstream from the target position, was used to deflect the beam to the left of the standard zero-degree line such that the centroid of the pion beam passed through the center of the polarized target when the target magnet was turned on. The beam spot on target was about 2.5 cm wide and 1.5 cm high. The position of the centroid of the beam relative to the center of the target cell was checked by creating an image of the target cell on a Polaroid film illuminated with the pion beam. This picture displayed shadows of the cylindrical walls of the copper cavity.

C. Large acceptance spectrometer (LAS)

The scattered particles were detected by the LAS [21, 22]. This spectrometer consists of two quadrupole magnets followed by a 45° bending magnet. The positions and angles of the particle trajectories were determined before and after the bender by a total of four sets of multiwire drift chambers, each containing position-sensitive wire planes that determine the horizontal and vertical positions of the passing particles.

The information from the wire chambers was used to calculate the scattering angle, the x and y coordinates of the reaction vertex (in a projection on the plane perpendicular to the optical axis of the spectrometer and inter-

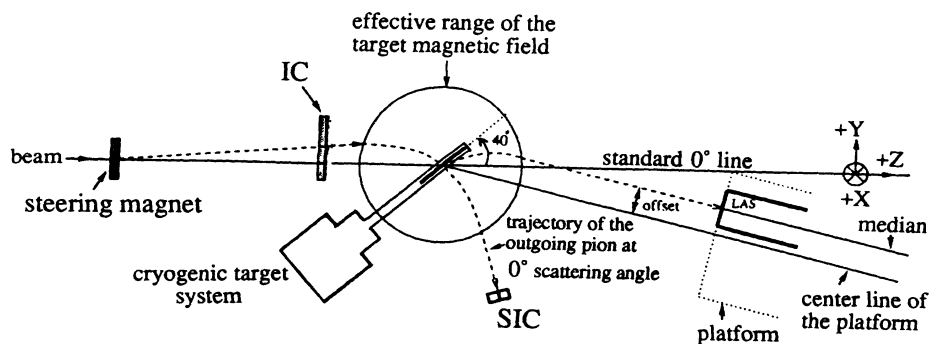


FIG. 1. Sketch of experimental setup. The trajectory of a typical pion ray is shown.

secting the center of the target), the momentum of the detected particle and thus the “missing mass” of the reaction. Two plastic scintillators placed behind the last wire chamber were used for particle identification by time-of-flight and energy loss.

The spectrometer was set up and optimized using calibration targets with the target magnet switched off. The momentum dependence of the spectrometer acceptance was obtained by measuring yields from a reaction of known cross section at different settings of the spectrometer magnets. We used pion inelastic scattering [23] to the $^{12}\text{C}(2^+, 4.44 \text{ MeV})$ state at $T_\pi = 226 \text{ MeV}$ and $\theta_{\text{lab}} = 27.5^\circ$, where the angular distribution has a maximum.

Ray-trace calculations were used to determine the necessary modifications to the LAS setup for data taking when the target magnet is switched on. These modifications included a horizontal shift (offset) of the whole spectrometer perpendicular to its median plane (Fig. 1). The distance that the spectrometer had to be shifted depended on the momentum of the scattered pions, and thus needed to be adjusted for each angle and energy change.

During the experiment, when the refrigerator system was fully operational, it was discovered that the center

of the target cell was actually 1 cm downstream from the center of the target magnet. As a consequence, the $\int B_m dl$ of the field of the target magnet (B_m) integrated from outside the field to the target position, is different for incoming and outgoing pions. For pions scattered from hydrogen a -2° correction to the scattering angle was calculated to result from the 1-cm shift. For pions scattered from ^{13}C the correction was small ($\sim 0.5^\circ$) compared to the angular resolution, because of the smaller momentum difference between incident and scattered pions and, thus, was neglected.

The 8° angular acceptance of LAS can be subdivided into smaller angular bins. However, the total angle of deflection in the target magnet varies with the unknown z coordinate of the reaction vertex in the polarized target. Therefore the angular resolution of the spectrometer is worsened to 2.8° from its normal value of 1.3° .

Typical missing mass spectra obtained at $T_\pi = 130 \text{ MeV}$ and $\theta_{\text{lab}} = 60^\circ$ are presented in Fig. 2. The energy resolution with the polarized target was limited to about 3 MeV(FWHM) by target thickness and inhomogeneity (bead structure). Spectra of better resolution, typically 1.4 MeV(FWHM), were obtained with an (unpolarized) ^{13}C slab target of 200 mg/cm^2 thickness. Figure 3 shows such a spectrum taken at $T_\pi = 130 \text{ MeV}$ and $\theta_{\text{lab}} = 60^\circ$. These spectra served to estimate contributions from excited states in the region of the elastic peak in the polarized target spectra and to obtain differential cross sections (see Sec. II F).

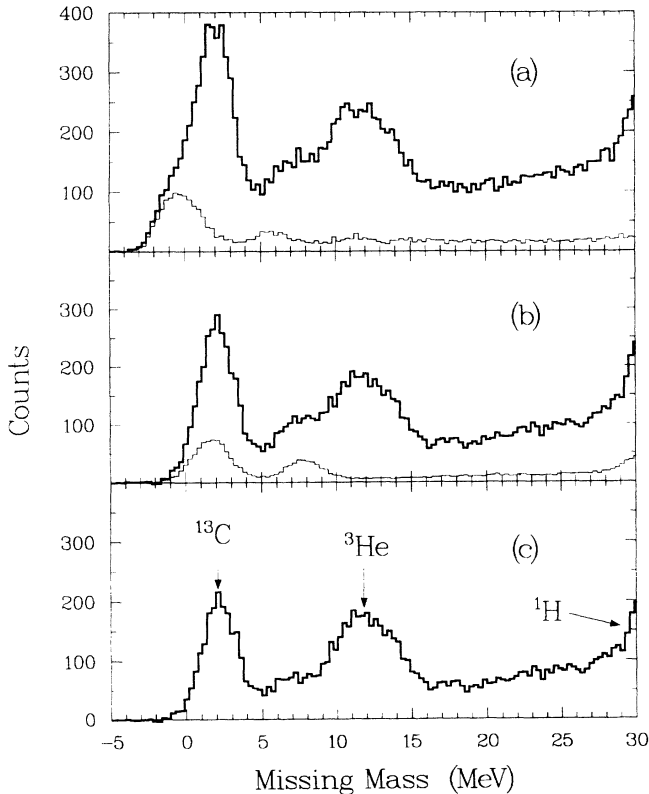


FIG. 2. Typical foreground and background-subtracted missing-mass spectra for pion scattering from $^{13}\text{C}_4\text{H}_{10}\text{O}$; (a) thick line: full spectrum; thin line: background spectrum from copper cavity; (b) thick line: spectrum with copper background subtracted; thin line: oxygen background spectrum; (c) thick line: spectrum with copper and oxygen background subtracted.

D. Background measurements

A replica of the cryogenic target, without the beads and ^3He coolant, was used to measure background yields. The normalized missing-mass spectrum of the replica target [the thin line in Fig. 2(a)] provides a background spectrum of all contaminants near the ^{13}C peak except for the events from the ^{16}O in the 1-butanol beads. The events from the ^3He coolant are kinematically separated

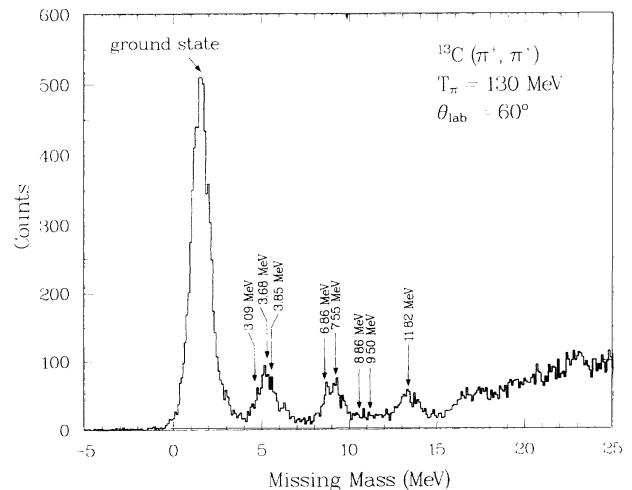


FIG. 3. Missing-mass spectrum for π^+ scattering on the ^{13}C graphite slab target at $\theta_{\text{lab}} = 60^\circ$ and $T_\pi = 130 \text{ MeV}$.

from the elastic ^{13}C peak.

The ^{16}O background [the thin line in Fig. 2(b)] was extracted from the difference of the replica spectrum and another spectrum using the replica target filled with distilled water. The ratio of the number of ^{16}O scattering centers in the water target to that in the cryogenic target was determined by measuring the ratio of cross sections for pions scattered from ^1H in the water target and in the unpolarized cryogenic target. This was done at 45° where the $\pi^{-1}\text{H}$ scattering yields are well separated kinematically from yields of other nuclei. For different channel settings, the size and the position of the beam spot on the target changes slightly. Thus the value of the extracted ratio of oxygen scattering centers in the cryogenic and water targets varied from 0.06 to 0.09. A missing-mass spectrum with both the background and oxygen contaminants subtracted is shown in Fig. 2(c).

E. Analyzing power measurements

In terms of measurable quantities, the analyzing power of pion scattering from polarized ^{13}C is

$$A_y = \frac{Y_\uparrow - Y_\downarrow}{(Y_\uparrow - B)P_\downarrow + (Y_\downarrow - B)P_\uparrow} = \frac{D}{S}. \quad (4)$$

Here P_\uparrow and P_\downarrow are the transverse polarizations of the ^{13}C target with spin orientation parallel (spin-up) and antiparallel (spin-down) to the norm to the reaction plane. Y_\uparrow and Y_\downarrow are the corresponding scattering yields. The background B in the region of the elastic peak originated from the walls of the target (copper microwave cavity and Teflon cell) and from the oxygen in the target material. D and S are the difference and the sum of the spin-up and spin-down yields, respectively.

At 130 MeV, π^+ and π^- spectra were measured with the polarized target and the target replica in 10° intervals between 40° and 130° . At 223 MeV with π^+ and at 226 MeV with π^- , spectra were obtained in 10° intervals between 30° and 80° . These data were analyzed using two 4° -wide bins.

A survey was made across the resonance at $T_\pi = 114, 130, 145, 165, 180,$ and 226 MeV for π^- scattering at two scattering angles, in order to search for predicted large A_y at momentum transfers (q) near the second minimum of $d\sigma(\theta)/d\Omega$. Here the momentum transfer was kept approximately constant by decreasing the scattering angle as the incident energy was increased. These data were analyzed using three 2.8° -wide bins.

Typical runs consisted of four parts, each about 2 h long. Runs would start with, e.g., spin-up, continue for two periods of spin-down, and end with one period with spin-up. This procedure should reveal false asymmetries, e.g., due to beam fluctuations on the target, but none were found.

Spectra of D and S were generated. Figure 4 shows these spectra, analyzed in ^{13}C kinematics, for π^- scattering, at $T_\pi = 130$ MeV and $\theta_{\text{lab}} = 60^\circ$. The difference is large in the region of the elastic peak of ^{13}C . A small difference can be seen in the region of the tail of the broad peak from elastic scattering on ^1H (missing mass ≈ 25

MeV). When replayed with ^1H kinematics, this peak is much more narrow as seen in the D and S spectra acquired at 54° with π^+ at $T_\pi = 130$ MeV (Fig. 5). Note that the yield in the D spectrum in the region of the elastic ^3He peak is 0 as expected. Because the background near the ^1H peak is structureless, a constant background was assumed and subtracted when generating the S spectra. For $\pi^{-1}\text{H}$ the A_y were obtained at 130 MeV and 223 MeV with π^+ , and at 226 MeV with π^- (Table I).

These measured values of A_y for $\pi^{-1}\text{H}$ scattering can be compared with the values of A_y calculated using the fitted phase shifts [24]. Within the error bars of both our measurement and the phase shift analysis, our $\pi^{-1}\text{H}$ analyzing powers are in agreement with the phase shift results (Table I). This result verifies the target polarizations obtained from the NMR measurements.

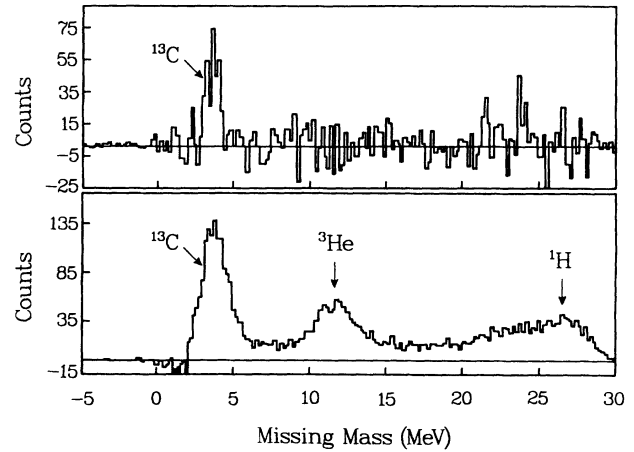


FIG. 4. D (top) and S (bottom) spectra for $^{13}\text{C}(\pi^-, \pi^-)$ at $\theta_{\text{lab}} = 60^\circ$ and $T_\pi = 130$ MeV.

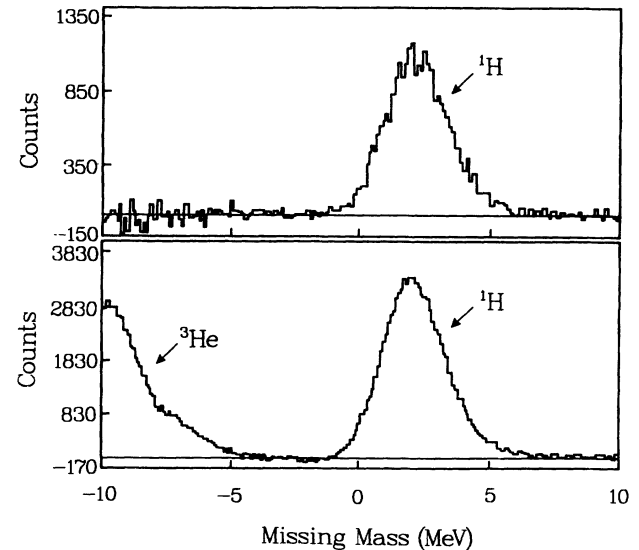


FIG. 5. D (top) and S (bottom) spectra with ^1H kinematics in the region of the $\pi^+{}^{-1}\text{H}$ peak at $\theta_{\text{lab}} = 54^\circ$ and $T_\pi = 130$ MeV.

TABLE I. Analyzing powers for $\pi^{-1}\text{H}$ elastic scattering from this experiment and predicted values from phase shifts [24].

Beam	T_π (MeV)	$\theta_{c.m.}$ (deg)	$A_y \pm \Delta A_y$ This experiment	$A_y \pm \Delta A_y$ Phase shift
π^+	130	54.3	$+0.331 \pm 0.005$	$+0.332 \pm 0.006$
π^+	223	51.6	$+0.235 \pm 0.005$	$+0.230 \pm 0.002$
π^-	226	50.3	-0.275 ± 0.016	-0.300 ± 0.010

$$\Delta A_y^i = \frac{|P_\uparrow + P_\downarrow| \sqrt{(Y_\downarrow - B)^2 (\Delta Y_\uparrow)^2 + (Y_\uparrow - B)^2 (\Delta Y_\downarrow)^2 + (Y_\uparrow - Y_\downarrow)^2 (\Delta B)^2}}{[Y_\uparrow P_\downarrow + Y_\downarrow P_\uparrow - B(P_\uparrow + P_\downarrow)]^2} \quad (6)$$

Here [with superscripts i omitted] $\Delta Y_\uparrow = \sqrt{Y_\uparrow}$ and $\Delta Y_\downarrow = \sqrt{Y_\downarrow}$ are the statistical errors of Y_\uparrow and Y_\downarrow . The quantities B and ΔB are the background yields and the background uncertainties given by the statistical errors in the replica target and water target runs.

The A_y were then obtained as the statistically weighted average of A_y^i :

$$A_y = \frac{\sum_{i=i_{\min}}^{i_{\max}} \frac{A_y^i}{(\Delta A_y^i)^2}}{\sum_{i=i_{\min}}^{i_{\max}} \frac{1}{(\Delta A_y^i)^2}} \quad (7)$$

and the uncertainty of A_y was calculated with

$$\Delta A_y = \frac{1}{\sqrt{\sum_{i=i_{\min}}^{i_{\max}} \frac{1}{(\Delta A_y^i)^2}}} \quad (8)$$

Here i represents the channel number within the specified lower (i_{\min}) and upper limits (i_{\max}). One advantage of this method is that the region of averaging can be varied in order to check for the effect of contributions to the elastic yield from the tails of the 3.09 MeV state and the 3.68/3.85 MeV doublet of ^{13}C .

The S spectra were used to determine the region over which the average A_y was to be calculated for the elastic peak. The upper limits (i_{\max}) were chosen conservatively in order to include only very few events from the excited states. The spectra from the slab target runs (see Fig. 3 and Sec. IIF) were used to provide information on the yield from the nearby triplet of states (3.09/3.68/3.85 MeV). Consistent results within error bars were attained when A_y was calculated either from the channels within the half-width of the elastic peak or slightly larger regions.

A systematic uncertainty of A_y results from the normalization of the water-filled target for background subtraction. The ratio of ^{16}O scattering centers in the water target to that in the polarized target was measured at only one angle (45°). Data at large angles were acquired

The asymmetries and the statistical uncertainties in A_y for the ^{13}C data were extracted by first creating spectra of A_y and its uncertainty, ΔA_y , from normalized spin-up, spin-down, and background missing-mass spectra. The values of A_y^i and ΔA_y^i for each missing-mass channel i of width 10 keV were calculated by

$$A_y^i \equiv \frac{D^i}{S^i} = \frac{Y_\uparrow - Y_\downarrow}{Y_\uparrow P_\downarrow + Y_\downarrow P_\uparrow - B(P_\downarrow + P_\uparrow)} \quad (5)$$

and

several days after the small-angle data. Therefore, the beam spot on the target may have changed, producing a different ratio than at the small angle. To investigate the effect of possible variations in the ratio, its value was artificially varied by up to 20%. This variation causes a change in A_y much less than the statistical uncertainty ΔA_y .

The analyzing powers of this work are presented in Figs. 7-12 in Sec. III with theoretical predictions. Nonzero analyzing powers were observed for π^- scattering at $T_\pi = 130$ MeV at angles near the first ($\simeq 60^\circ$) and second minimum ($\simeq 100^\circ$) of $d\sigma/d\Omega$ (Fig. 7). For π^+ scattering, the A_y values are consistent with 0 at all angles. A larger A_y is expected and observed for π^- scattering than for π^+ scattering because ^{13}C has an excess neutron to which π^- couple more strongly than π^+ in the region of the P_{33} resonance [25]. The A_y for π^+ at $T_\pi = 223$ MeV and for π^- at $T_\pi = 226$ MeV are shown in Fig. 8. At these energies above the resonance, A_y were found to be consistent with 0 for both π^+ and π^- in the angular range of $40^\circ - 80^\circ$.

The analyzing powers for π^- scatterings at the momentum transfer near the second minimum of $d\sigma/d\Omega$ were found to be very small at all energies (Fig. 9). Especially at $T_\pi = 165$ MeV our data are consistent with 0, a result similar to that observed in the experiment [6, 8] on $^{15}\text{N}(\pi^+, \pi^+)$ at 164 MeV. The six data points at $T_\pi = 130$ MeV in Fig. 9 were obtained from two runs that were analyzed with three angular bins each. The same data analyzed in two angular bins are presented in the angular distribution (Fig. 7) as four data points between 100° and 115° .

The error bars of the asymmetry data shown in the figures are the statistical errors multiplied by 1.12 to account for the effect of the uncertainty in the missing-mass range over which the weighted average A_y was obtained. The 3% systematic uncertainty in the polarization measurement is neglected.

F. Differential cross-section measurements

Differential cross sections for pion elastic scattering from unpolarized ^{13}C were obtained using a graphite slab enriched in ^{13}C to 99%. For most runs with this target,

the target magnet was turned on in order to provide reference spectra (Fig. 3) of better energy resolution for comparison with the cryogenic target spectra.

Absolute differential cross sections were calculated by normalizing the yields from the ^{13}C slab target to yields from a CH_2 target. The cross sections for ^{12}C were taken from the literature [23, 26, 27] or, at energies where no data exist, calculated using an optical-model program [28]. (Existing ^{12}C data at many energies were fitted well by these calculations.)

At 130 MeV, spectra were also taken with π^+ with the target magnet turned off at some angles for comparison with the $d\sigma(\theta)/d\Omega$ obtained when the target magnet was turned on. For several spectra, taken with the target magnet turned off, we have also obtained an absolute normalization using the yields from scattering by the hydrogen in the CH_2 target and the calculated cross section from a phase shift fit to existing data [24]. There is good agreement between the data obtained with the magnetic field turned on and turned off.

At 130 MeV, the $^{13}\text{C}(\pi^\pm, \pi^\pm)$ yields at $\theta_{\text{c.m.}} = 42^\circ$ were also measured (with the target magnet turned on), using the unpolarized cryogenic target. Both the π - ^{13}C and π - ^1H peaks were seen in the missing-mass spectrum. Again the π - ^1H yields and the known cross sections for π -p scattering [24] were used to obtain the absolute cross sections of $^{13}\text{C}(\pi^\pm, \pi^\pm)$. However, the absolute cross section deduced from the π^+ run (the square in the top right panel of Fig. 7) is about 25% lower than that from the slab target runs which were normalized to the ^{12}C cross sections. This discrepancy was not observed for π^- and is not understood.

The differential cross sections are presented in Sec. III with the experimental asymmetries and theoretical calculations in Figs. 7, 8, and 10–12. Generally, the systematic uncertainties in the normalization and thus in the absolute cross sections are 10–20% at forward angles (less than 65°) and as large as 50% at larger angles. The error bars in Fig. 7, for instance, are the statistical uncertainties only and do not include these systematic uncertainties. Our data at 165 MeV (not shown) are in good agreement with the detailed angular distribution of Ref. [11] at 162 MeV. Whereas the large systematic uncertainties in some of the cross-section data are not satisfactory, we point out that the analyzing powers, which were the primary goal of this experiment, are not affected by the normalization uncertainties.

III. THEORETICAL ANALYSIS OF THE DATA

A. General remarks

Measurements of the analyzing power in pion scattering and single charge exchange (SCX) reactions provide information on nuclear spin transitions and the pion-nucleus reaction dynamics. Theoretical analyses [4–8, 17–19, 29, 30, 33, 34] using different nuclear structure and

pion-nucleus reaction models have thus far not been successful in reproducing the data for ^6Li , ^{13}C , and ^{15}N . Only the very recent data [31] on ^3He at 100 MeV have been reproduced by theory. However, it was found [32] that the analyzing power for ^3He at the incident energy of 100 MeV is insensitive to the nuclear structure input and the approximations used in the calculations whereas at energies above about 150 MeV, higher-order terms in the reaction model and the small components in the nuclear wave function are predicted to be important.

The failure of theory to reproduce the data for ^{13}C and ^{15}N may be due to a lack of understanding of either the pion-nucleus dynamics or the nuclear spin transition density, or both. Below we demonstrate the strong sensitivity of the analyzing power to the details of the nuclear spin transition density. We also present a variety of theoretical calculations using different models for the elastic-scattering process. An independent analysis of our data by Siegel and Gibbs [33] has recently been published.

Our current understanding of the spin-dependent part of the nuclear transition structure has been tested by comparison of the magnetic form factor $|F_{M1}|^2$ extracted from electron scattering with theoretically predicted $|F_{M1}|^2$. $^{13}\text{C}(e, e)$ data exist [12] over a large range of momentum transfers (Fig. 6). The solid line in this figure is the theoretical $|F_{M1}|^2$ calculated by us with the code ALLWORLD [36]. We used the transition densities calculated by Lee and Kurath (LK) [16] in the model of Cohen and Kurath (CK) [15] (hereafter referred to as CK-LK transition densities). The squares of the isoscalar (isospin transfer $\Delta T=0$) and isovector ($\Delta T=1$) parts of the magnetic form factor amplitudes are shown as dotted and dashed lines, respectively. The $\Delta T=1$ part dominates at large momentum transfers, $q \geq 1.5 \text{ fm}^{-1}$. At $q \approx 0.6 \text{ fm}^{-1}$, the $\Delta T=0$ and $\Delta T=1$ parts are comparable in magnitude. The square of the $\Delta T=1$ spin part (without the convection current terms) (chain-dotted line) is a factor of $(\mu_p - \mu_n)^2 / (\mu_p + \mu_n)^2 = 28.5$ larger than that of the $\Delta T=0$ spin part (chain-dashed line). Here μ_p (μ_n) is the proton (neutron) magnetic moment. The coherent addition of the spin and current terms results in the above-mentioned different q -dependences of the $\Delta T=0$ and $\Delta T=1$ parts of $|F_{M1}|^2$ and a good fit to the experimental $|F_{M1}|^2$ up to $q \approx 1.3 \text{ fm}^{-1}$.

The analyzing power in pion scattering has an isospin sensitivity very different from that of $|F_{M1}|^2$. In the region of the $P_{3,3}$ resonance, the ratio r of the $\Delta T=0$ and $\Delta T=1$ pion-nucleus scattering amplitudes is, independent of q , $r = +2$ for π^- and $r = -2$ for π^+ if protons and neutrons contribute equally to the transition and if first-order processes dominate. Terms analogous to the current terms in electron scattering are thought to be small in pion scattering.

Because of this very different isospin dependence of the spin transitions in electron and pion elastic scattering, the pion A_y values provide information complementary to the magnetic form factor for comparison with nuclear model predictions, especially for the $\Delta T=0$, $\Delta S=1$ part of the transition density. We note that pion-induced SCX reactions [18] proceed exclusively by the isovector parts of $\mathcal{F}(\theta)$ and $\mathcal{G}(\theta)$.

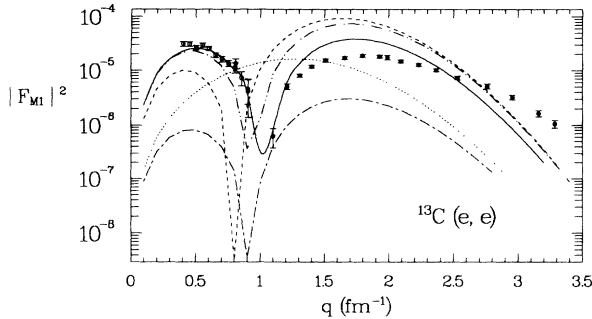


FIG. 6. Magnetic form factor squared, $|F_{M1}|^2$. Data of Ref. [12] for $^{13}\text{C}(e, e)$. Solid line: prediction with program ALLWORLD [36] using CK-LK [15, 16] densities. Dotted (dashed) line: $\Delta T=0$ ($\Delta T=1$) parts; chain-dashed: $\Delta T=0$, spin part only; chain-dotted: $\Delta T=1$, spin part only.

B. Distorted wave impulse approximation analysis

We calculated A_y using a model which employs a first-order optical potential [34]. We used the optical-model program PIPIT [35] (which does not include spin transfer) in conjunction with the inelastic-scattering code ARPIN [16]. The spin-independent and spin-dependent parts of the elastic transition amplitude were obtained from ARPIN. The $d\sigma/d\Omega$ and A_y were calculated in the distorted wave impulse approximation (DWIA) with the distorted waves from PIPIT. The pion-nucleon t -matrix was calculated at an energy below the actual pion-nucleon center-of-mass energy. This energy shift appears to correct for some second-order effects. We found that at $T_\pi = 130$ MeV an energy shift of 12 MeV for π^+ and of 8 MeV for π^- gave better fits to the elastic scattering cross sections than the 20 MeV shift used [11] at 162 MeV. The difference of 4 MeV between the values for π^+ and π^- approximately accounts for the π -nucleus Coulomb energy differences at the nuclear surface. A Gaussian off-shell model [35] was employed with a momentum range parameter [34, 35] of $3 \times 10^{-6} \text{ MeV}^{-2}$ at all energies.

The nuclear transition density amplitudes are usually classified [16] according to the total and the orbital angular momentum transfers J and L , and the spin transfer S . Specifically, for elastic scattering on a spin-1/2 nucleus such as ^{13}C , there are three possible combinations (Table II) of $J(LS)$: 0(00), 1(01), and 1(21), since the $L = 1$ terms can be neglected in a first-order calculation. In terms of the nuclear transition amplitudes, the pion-nucleus amplitude $\mathcal{F}(\theta)$ is proportional to the 0(00) part and $\mathcal{G}(\theta)$ is proportional to a combination of the 1(01) and 1(21) parts.

The elastic scattering cross sections and analyzing powers were calculated by combining the $J = 0$ scattering amplitude from a first-order optical potential using PIPIT [35] with the $J = 1$ scattering amplitudes from a DWIA calculation using ARPIN [16]. Shell-model transition densities (Table II) of CK, LK [15, 16], and of Tiator

and Wright (TW) [37] and variations of these densities were employed.

The CK-LK densities [16] were constructed using the effective interaction for the $1p$ shell obtained by fitting energy levels of nuclei from $A = 6$ to $A = 16$ [15]. The TW density was obtained [38] using the experimental magnetic moments of $A = 13$ nuclei, the β decay constant of ^{13}N , and the magnetic form factor of ^{13}C as input. Since the quadrupole spin-flip [$J(LS) = 1(21)$] transition is not uniquely determined by the above inputs [38], its transition amplitude was obtained by minimizing the contribution of the $M1$ transition to the $^{13}\text{C}(\gamma, \pi^-)$ cross sections [39].

C. Comparison with experimental data

At $T_\pi = 130$ MeV, the predictions to the elastic differential cross sections are presented in Fig. 7 (top). The choice of either the CK-LK or TW densities has only a very small effect on $d\sigma/d\Omega$, which is dominated by the 0(00) amplitudes (identical for CK-LK and TW). The analyzing powers (bottom of Fig. 7) are very different for CK-LK (solid lines) and TW (dashed lines).

In general, the DWIA calculations with CK-LK densities give a poor description of the π^- analyzing power data. Whereas the experiment gives positive A_y between $\theta_{c.m.} = 40^\circ$ and 95° , the theoretical A_y with the CK-LK density change sign in the region from negative at small angles to positive at 53° and then back to negative at 82° with $A_y(\text{theory})$ reaching about -1.0 at 98° (solid lines in Fig. 7). In this large-angle region experimental and theoretical A_y with the CK-LK density are out of phase.

We note that at angles smaller than 70° (momentum transfer $q \approx 1.3 \text{ fm}^{-1}$) the Cohen-Kurath model [15] provides us with reliable ground state (g.s.) spin transition densities. The disagreement between the pion data and theory is the largest at $80^\circ < \theta_{c.m.} < 96^\circ$ ($1.5 \text{ fm}^{-1} < q < 1.7 \text{ fm}^{-1}$), where the A_y depend

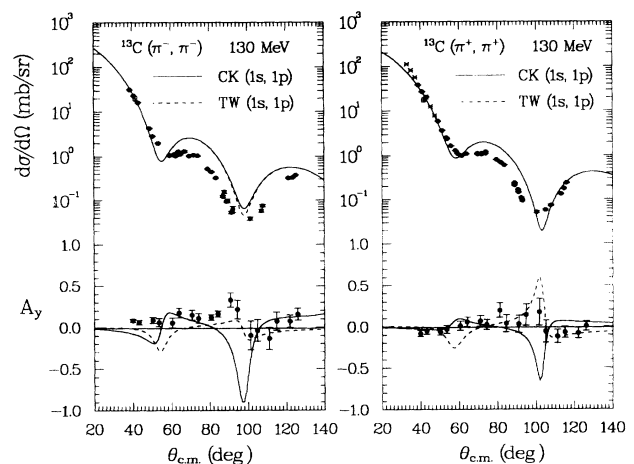


FIG. 7. $d\sigma/d\Omega$ and A_y of $^{13}\text{C}(\pi, \pi)$ at 130 MeV. The DWIA calculation with CK-LK [15, 16] (TW [37]) densities are shown as solid (dashed) line.

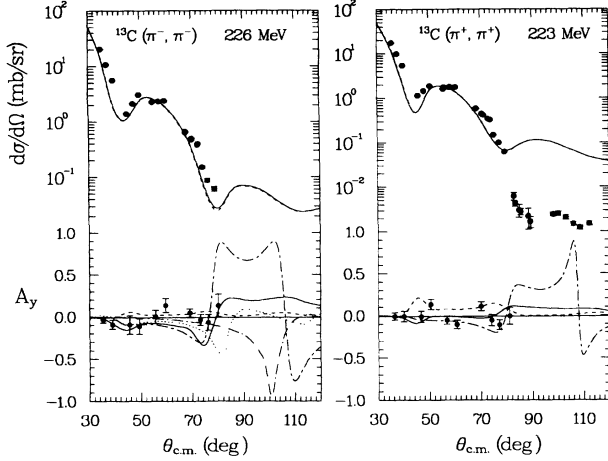


FIG. 8. $d\sigma/d\Omega$ and A_y of $^{13}\text{C}(\pi^-, \pi^-)$ at 226 MeV and of $^{13}\text{C}(\pi^+, \pi^+)$ at 223 MeV. The curves were obtained from calculations by Mach [5] using the CK-LK density [15, 16] (solid line) and the TW density [37] (dashed line), from the full Δ -hole model [4] prediction (dotted line), from the calculation in the closure approximation to the Δ -hole model (chain-dotted line), and from this work using the CK-LK density (chain-dashed line).

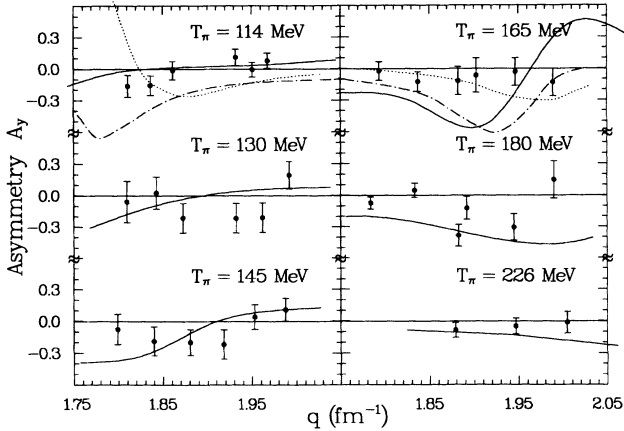


FIG. 9. A_y of $^{13}\text{C}(\pi^-, \pi^-)$ at energies across the P_{33} resonance at momentum transfers (q) near the second minimum of the differential cross sections. The curves at 114 MeV and 165 MeV are the predictions of Thies using the Δ -hole model [4] (dotted lines) and the closure approximation to this model (chain-dotted). The solid lines are calculations of Mach [5] with CK-LK [15, 16] densities.

strongly on both the reaction mechanism and the nuclear structure model. In addition, standard nuclear structure models have thus far failed to reproduce the measured magnetic form factor [12] at $q > 1.3 \text{ fm}^{-1}$. The π^+ analyzing power data are consistent with zero at all angles but the CK-LK density predicts large negative A_y near 90° .

The TW density had been designed to fit the anomalous $^{13}\text{C}(\gamma, \pi^-)$ cross sections [39]. DWIA calculations

with these densities (Fig. 7, dashed lines) fail to fit the π^- analyzing power data by predicting either negative (near 50°) or near zero A_y (at 90°) whereas the data are either positive at intermediate angles or consistent with zero at small and large angles. What may be interpreted as a fit to the π^+ data near 90° with the TW densities is probably fortuitous since the data at small angles do not show the predicted negative analyzing power.

We note that the CK-LK and TW transition density amplitudes are very similar for 1(01) but totally different for 1(21) (Table II). What is primarily a 1(21) neutron particle-hole (p-h) amplitude in CK-LK is almost a pure proton p-h amplitude in TW. We have therefore studied how A_y is affected by renormalizing the quadrupole spin-flip [1(21)] amplitude by a factor α . The solid line in Fig. 10 shows again the calculated A_y with the 1(21) value of CK-LK. Arbitrarily changing the sign of the 1(21) amplitude essentially flips the sign of the analyzing power (dashed line). Using two times the CK-LK value nearly doubles A_y (chain-dashed line). Making the 1(21) piece zero gives a very small A_y (dotted line), which arises only from the interference of the 0(00) and 1(01) amplitudes. Thus A_y is exceedingly sensitive to the quadrupole spin-flip term. However, it appears that no value of the 1(21) amplitude would fit the data with the 0(00) and 1(01) parts left unchanged.

It was shown by Hicks *et al.* [12] that the fit to $|F_{M1}|^2$ at high q can be much improved by including a 16% admixture of higher-shell ($2\hbar\omega$) components in the nuclear wave functions. In order to explore the effects on A_y of including higher shell admixtures, we have also done calculations with the phenomenological wave functions of Ref. [40] which contain both $1p$ and $2p$ shell contributions. We find (Fig. 11) that for both π^- and π^+

TABLE II. Neutron $\langle n \rangle$ and proton $\langle p \rangle$ parts of transition density amplitudes.

	J(LS)	0(00)	1(01)	1(21)
CK-LK	$\langle n \rangle$	2.041	-0.235	0.929
Ref. [16]	$\langle p \rangle$	1.633	-0.003	0.039
TW	$\langle n \rangle$	2.041	-0.208	-0.096
Ref. [37]	$\langle p \rangle$	1.633	-0.015	-0.516

the $2p$ admixtures reduce the analyzing power near the first diffraction minimum but increase it near the second one with no improvement in the fit to the data. Relatively larger effects from the $2p$ admixtures were found in DWIA calculations for SCX [41].

Before conclusions can be drawn from the analyzing powers about the validity of nuclear wave functions, the pion-nucleus reaction model needs to be understood better. With the CK-LK densities, Mach [5] provided a prediction (solid lines in Fig. 9 and Fig. 12), based on a first-order optical potential as above, but including a phenomenological ρ^2 term which was adjusted to fit $d\sigma/d\Omega$ at various energies. Here ρ is the nuclear density. Mach's predictions yield values of A_y similar to those of our calculations but fit better at $\theta_{c.m.} \approx 55^\circ$. The fits to the A_y

data for both π^+ and π^- near 100° are still not satisfactory.

Additional calculations (dashed lines in Fig. 12) were performed by Mach with the same reaction model, but with densities provided by Tiator [37, 38]. The DWIA curves from these calculations disagree with the data at larger angles for π^- . For π^+ a small peak predicted at 95° is consistent with the data, although the error bars do not rule out zero A_y .

The small A_y observed in the energy-dependence data and some predictions are shown in Fig. 9. At 165 MeV the data disagree with the curve obtained with CK-LK [16, 15] densities by Mach (solid lines) and a very similar one obtained by us (not shown). Δ -hole model predictions of Thies [4] are also available at some of these energies and shown as dotted lines (full calculation) and chain-dotted lines (closure approximation). The wave functions used in these two Δ -hole calculations are again different from those of CK-LK and TW. But the large difference in the predicted A_y (Fig. 9) from two different approaches to the reaction mechanism shows that the A_y are sensitive to the reaction model. At 165 MeV, the data show a preference for the full calculation. Δ -hole model calculations are not yet available at the other energies.

At 226 MeV, the analyzing powers predicted by the Δ -hole model are very different from those of Mach and of this work (Fig. 8), especially at angles greater than 80° . However, our data at 226 MeV for π^- and 223 MeV for π^+ cannot distinguish between different interaction models. Because of the exceedingly small cross section at angles greater than 80° , the A_y measurements at these energies could be done only at angles smaller than 80° . Unfortunately, at $T_\pi = 130$ MeV, where a wide angular distribution of $d\sigma/d\Omega$ and A_y was measured in this experiment, Δ -hole model calculations are not yet available. Such calculations are needed at all the energies of this experiment.

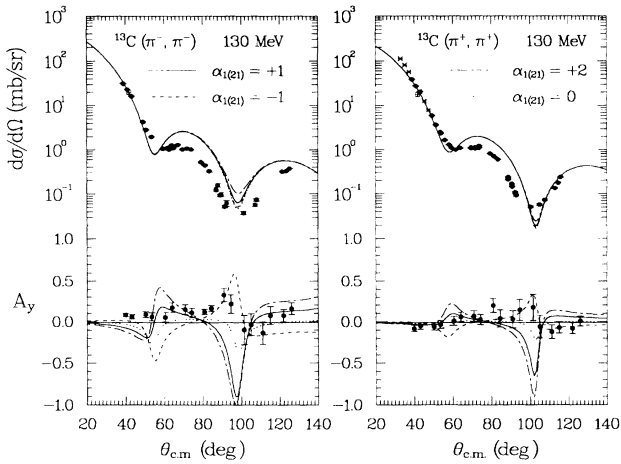


FIG. 10. $d\sigma/d\Omega$ and A_y of $^{13}\text{C}(\pi, \pi)$ at 130 MeV. Solid line: DWIA calculation with CK-LK [15, 16] densities and variations of a factor, α , on the quadrupole spin-flip transition amplitude, $J(LS) = 1(21)$.

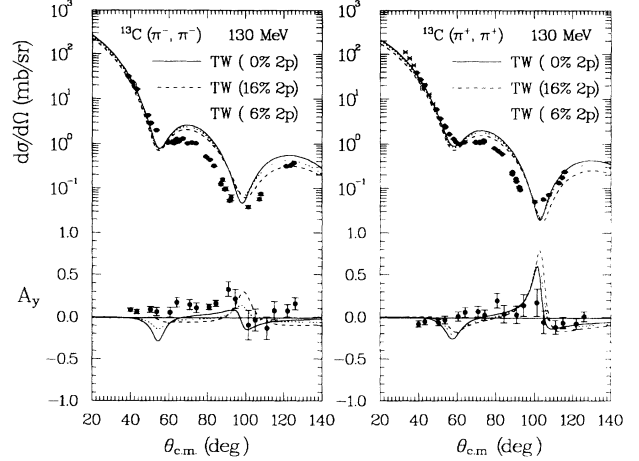


FIG. 11. $d\sigma/d\Omega$ and A_y of $^{13}\text{C}(\pi, \pi)$ at 130 MeV. Solid line: DWIA calculation with TW [37] densities. Dashed (dotted) line: with 16% (6%) $2p$ -shell admixture.

IV. SUMMARY

Analyzing powers and differential cross sections were measured for π^+ and π^- elastic scatterings on ^{13}C . A polarized cryogenic target using ^{13}C -enriched 1-butanol beads was employed. The differential cross sections were measured using a ^{13}C -enriched graphite target. Angular distributions of both A_y and $d\sigma/d\Omega$ were obtained below the P_{33} resonance at 130 MeV for π^+ and π^- , and above the resonance at 223 MeV for π^+ and at 226 MeV for π^- . In addition, A_y and $d\sigma/d\Omega$ were measured in a range of momentum transfers, $1.75 \leq q \leq 2.05 \text{ fm}^{-1}$, at several energies (114, 145, 165, and 180 MeV). At $T_\pi = 130$ MeV, the values of A_y are different from zero for π^- scattering. For π^+ at $T_\pi = 130$ MeV and for both π^- and π^+ at all other energies, the A_y are mostly consistent with zero.

Being sensitive to the isoscalar part of the nuclear transition, the pion data complement measurements of the

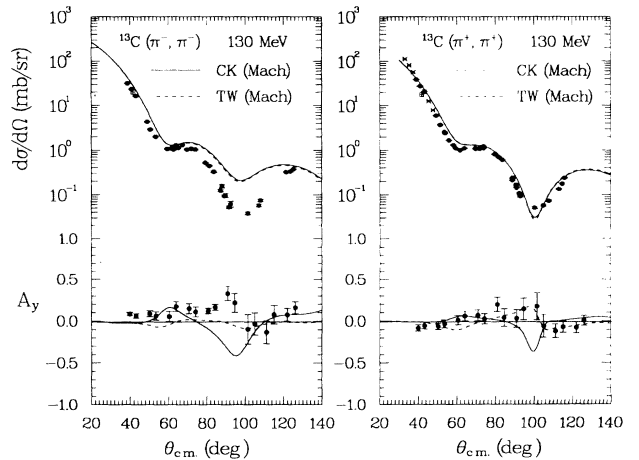


FIG. 12. $d\sigma/d\Omega$ and A_y of $^{13}\text{C}(\pi, \pi)$ at $T_\pi = 130$ MeV. The curves were obtained from calculations by Mach [5] using CK [15, 16] (solid line) and TW [37] (dashed line) densities.

(isovector-dominated) magnetic form factor from electron scattering. Calculations using different reaction models demonstrate a strong sensitivity of A_y to the reaction mechanism above the P_{33} resonance. Inclusion of a phenomenological ρ^2 term provides larger changes in the predicted A_y than in $d\sigma/d\Omega$.

Theoretical analyses were done using different nuclear structure models. The data were not reproduced by the presently available nuclear wave functions. It was found that the analyzing power is strongly sensitive to the $J(LS) = 1(21)$ (the quadrupole spin-flip) part of the transition. However, the A_y could not be reproduced by varying the spin-dependent nuclear transition amplitudes. It was also found that inclusion of higher shell admixtures, which give a better fit to the $|F_{M1}|^2$ data, does not improve the fit to A_y at high momentum transfer.

The analyzing power data of this and other similar work [6, 7] are not yet understood theoretically. They

contain new information on the nuclear spin transition density and the pion-nucleus reaction mechanism. Further effort is needed to describe the high- q behavior of the nuclear transition density, and specifically, its isoscalar spin-dependent part. Once that task is accomplished, our data may provide tests of pion-nucleus interaction theories which include higher-order terms such as the Δ -nucleus spin-orbit force.

ACKNOWLEDGMENTS

We thank Dr. R. Mach and Dr. M. Thies for permission to present the results of their theoretical calculations. We also acknowledge a grant for computing time from the Minnesota Supercomputer Institute. This work was supported in part by the U.S. Department of Energy, the University of Minnesota Graduate School, and the Robert A. Welch Foundation.

-
- [1] Proceedings of the LAMPF Workshop on Physics with Polarized Nuclear Targets, 1986, edited by G. R. Burleson, W. R. Gibbs, G. W. Hoffmann, J. J. Jarmer, and N. Tanaka [Los Alamos National Laboratory Report No. LA-10772-C (1986)].
- [2] J. J. Jarmer, S. I. Penttilä, D. Hill, T. Kasprzyk, M. Krumpolc, M. L. Barlett, G. W. Hoffmann, and L. Ray, Nucl. Instrum. Methods Phys. Res. Sect. A **250**, 576 (1986).
- [3] S. I. Penttilä *et al.*, in *Proceedings of the 9th International Symposium on High Energy Spin Physics*, edited by W. Meyer, E. Steffens, and W. Thiel (Springer-Verlag, Berlin, 1991), Vol. 2, pp. 315.
- [4] M. Hirata, F. Lenz, and M. Thies, Phys. Rev. C **28**, 785 (1983); M. Thies (private communication).
- [5] R. Mach and S. S. Kamalov, Nucl. Phys. **A511**, 601 (1990); R. Mach (private communication).
- [6] R. Tacik *et al.*, Phys. Rev. Lett. **63**, 1784 (1989).
- [7] S. Ritt *et al.*, Phys. Rev. C **43**, 745 (1991).
- [8] R. Meier *et al.*, Phys. Rev. C **42**, 2222 (1990).
- [9] D. Dehnhard, S. J. Tripp, M. A. Franey, G. S. Kyle, C. L. Morris, R. L. Boudrie, J. Piffaretti, and H. A. Thiessen, Phys. Rev. Lett. **43**, 1091 (1979).
- [10] S. J. Seestrom-Morris, D. Dehnhard, M. A. Franey, G. S. Kyle, C. L. Morris, R. L. Boudrie, H. A. Thiessen, and J. Piffaretti, Phys. Rev. C **26**, 954 (1982).
- [11] S. J. Seestrom-Morris, D. Dehnhard, M. A. Franey, G. S. Kyle, C. L. Morris, R. L. Boudrie, H. A. Thiessen, and J. Piffaretti, Phys. Rev. C **28**, 1301 (1983).
- [12] R. S. Hicks, J. Dubach, R. A. Lindgren, B. Parker, and G. A. Peterson, Phys. Rev. C **26**, 339 (1982).
- [13] S. J. Seestrom-Morris, M. A. Franey, D. Dehnhard, D. B. Holtkamp, R. L. Boudrie, J. F. Amann, G. C. Idzorek, and C. A. Goulding, Phys. Rev. C **30**, 270 (1984).
- [14] S. F. Collins, G. G. Shute, B. M. Spicer, V. C. Officer, D. W. Devins, D. L. Friesel, and W. P. Jones, Nucl. Phys. **A481**, 494 (1988).
- [15] S. Cohen and D. Kurath, Nucl. Phys. **73**, 1 (1965); **A226**, 253 (1974).
- [16] T.-S. H. Lee and D. Kurath, Phys. Rev. C **21**, 293 (1980).
- [17] J. T. Brack *et al.*, Phys. Rev. C **45**, 698 (1992).
- [18] J. J. Görden *et al.*, Phys. Rev. Lett. **66**, 2193 (1991).
- [19] Yi-Fen Yen *et al.*, Phys. Rev. Lett. **66**, 1959 (1991); Ph.D. thesis, University of Minnesota, 1991; Los Alamos National Laboratory Report No. LA-12373-T, UC-410, 1992; D. Dehnhard, Yi-Fen Yen, M. A. Franey, and S. Chakravarti, in *Proceedings of the 5th International Symposium on Mesons and Light Nuclei, Prague, September 1991*, edited by E. Truhlik and R. Mach [Few-Body Syst. Suppl. **5**, 274 (1992)].
- [20] A. G. Redfield, Phys. Rev. **98**, 1787 (1955); Science **164**, 1015 (1969).
- [21] E. Colton, Nucl. Instrum. Methods **178**, 95 (1980).
- [22] A. L. Williams *et al.*, Phys. Lett. B **216**, 11 (1989).
- [23] W. B. Cottingham *et al.*, Phys. Rev. C **36**, 230 (1987).
- [24] R. A. Arndt, J. M. Ford, and L. D. Roper, Phys. Rev. D **32**, 1085 (1985).
- [25] C. L. Morris *et al.*, Phys. Rev. C **17**, 227 (1978).
- [26] J. Piffaretti, R. Corfu, J.-P. Egger, P. Gretillat, C. Lunke, E. Schwarz, and C. Perrin, Phys. Lett. **67B**, 289 (1977).
- [27] J. Piffaretti, R. Corfu, J.-P. Egger, P. Gretillat, C. Lunke, E. Schwarz, C. Perrin, and B. M. Freedom, Phys. Lett. **71B**, 324 (1977).
- [28] Program DAMIT, E. V. Hungerford, Nucl. Instrum. Methods **111**, 509 (1973).
- [29] R. Mach and S. S. Kamalov, Nucl. Phys. **A511**, 601 (1990).
- [30] E. Boschitz, in *Proceedings of the 5th International Symposium on Mesons and Light Nuclei, Prague, September 1991*, edited by E. Truhlik and R. Mach [Few-Body Syst. Suppl. **5**, 191 (1992)].
- [31] B. Larson *et al.*, Phys. Rev. Lett. **67**, 3356 (1991).
- [32] S. S. Kamalov, L. Tiator, and C. Bennhold, Phys. Rev. C **47**, 941 (1993).
- [33] P. B. Siegel and W. R. Gibbs, Phys. Rev. C **48**, 1939 (1993).
- [34] S. Chakravarti *et al.*, University of Minnesota report, 1990 (unpublished).

- [35] R. A. Eisenstein and F. Tabakin, *Comput. Phys. Commun.* **12**, 237 (1976).
- [36] J. Carr, F. Petrovich, and J. Kelly, computer code ALLWORLD (unpublished).
- [37] L. Tiator and L. E. Wright, *Phys. Rev. C* **30**, 989 (1984).
- [38] L. Tiator, *Phys. Lett. B* **125**, 367 (1983).
- [39] P. C. Dunn *et al.*, *Phys. Lett. B* **196**, 434 (1987).
- [40] C. Bennhold and L. Tiator, *Phys. Lett. B* **238**, 31 (1990).
- [41] S. S. Kamalov, C. Bennhold, and R. Mach, *Phys. Lett. B* **259**, 410 (1991).

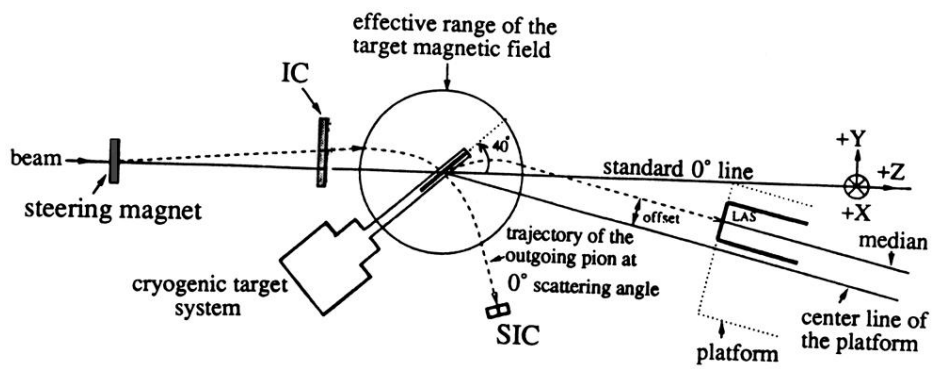


FIG. 1. Sketch of experimental setup. The trajectory of a typical pion ray is shown.